V European Conference on Computational Fluid Dynamics
ECCOMAS CFD 2010
J. C. F. Pereira and A. Sequeira (Eds)
Lisbon, Portugal,14-17 June 2010

EFFICIENT COMPUTATION OF DYNAMIC STABILITY DATA WITH A LINEARIZED FREQUENCY DOMAIN SOLVER

M. Widhalm*, R. P. Dwight*[1], R. Thormann† and A. Hübner††

*German Aerospace Center (DLR), Institute of Aerodynamics and Flow Technology.
Lilienthalplatz 7, 38108 Braunschweig.
markus.widhalm@dlr.de

†German Aerospace Center (DLR), Institute of Aeroelasticity,
Bunsenstr. 10, 37073 Göttingen
reik.thormann@dlr.de

††German Aerospace Center (DLR), Institute of Aerodynamics and Flow Technology.
Lilienthalplatz 7, 38108 Braunschweig.
andreas.huebner@dlr.de

Key words: unsteady aerodynamics, flutter analysis, linearization, frequency domain

Abstract. *Determination of aeroelastic stability boundaries for full aircraft configurations by solving the time-accurate unsteady Reynolds-averaged Navier-Stokes (RANS) equations is recognized as extremely computationally expensive or impractical. This is due to the wide range of flight conditions, frequencies, and structural deformation mode shapes that must be examined to ensure a configuration is free from flutter. Nonetheless there is an increasing demand within the aerospace industry for accurate flutter analysis in the transonic regime, which can only be satisfied with the use of high-fidelity RANS codes. Hence we are motivated to seek a more efficient numerical method. By assuming that perturbations to the flow are small and harmonic, we can derive an efficient alternative method by linearization of the RANS equations, a* linearized frequency domain *(LFD) solver. With this approach the unsteady simulation reduces to a single non-linear steady computation followed by a single linear simulation in the frequency-domain. This method is not new, but has principally been applied to turbomachinery so far. The contribution of this paper twofold: firstly to show that LFD is sufficiently accurate and reliable for applications to aeroelastic problems that occur in external aerodynamics, and secondly to demonstrate the speed-up that can be expected over full unsteady computations. Viscous transonic analysis is carried out on complex geometries in three-dimensions. The results show good agreement with full unsteady simulation and experiment, and a reduction in computational costs up to one order of magnitude is demonstrated.*

[1]Currently: TU Delft, Faculty of Aerospace, Aerodynamics Group, r.p.dwight@tudelft.nl.

1 INTRODUCTION

The design and development of transport aircraft tend towards increasing cruise velocity and lighter structures, and both together intensifies the influence of aeroelasticity which is especially important in the transonic flow regime. Flutter is a critical phenomena, and is defined as the transfer of energy from the flow to the structure in such as way as to amplify oscillations. It occurs particularly at high speeds and for flexible wings. It has an important role in aircraft design, and must be taken into account in the early stage of an aircraft development process, to prevent excessive structural loading and ensure safe flight operations.

In flutter analysis the main objective is to calculate the point at which the system becomes unstable, as function of various parameters, in particular Mach number and altitude. Performing non-linear unsteady simulations (URANS) in the time domain to obtain the aerodynamic loads is too expensive to cover the large parameter space spanned by flight conditions of interest, structural mode shapes and reduced frequency range. For subsonic flows small unsteady perturbations can be calculated independently by the superposition principle, because the governing flow equations are almost linear with respect to the motion. Thus efficient solvers for unsteady aerodynamics like the Doublet Lattice Method[1,3,11,19] (DLM) are used.

In the transonic regime the unsteady perturbations depend on the steady state and are in general neither linear nor harmonic. In addition, the flutter stability limit exhibits complex behavior (as typified by transonic dip) and can no longer be captured by linear methods like DLM. However, for small amplitudes the RANS equations can be linearized about the steady state and transformed into the frequency domain, solving directly for the first harmonic of the perturbation. The small perturbation assumption is justified by our principle interest in the linear stability behavior, which will be captured in the limit of infinitesimal displacements. The harmonic assumption requires that we investigate the stability of the system for a range of frequencies to eliminate the possibility of flutter at a given set of conditions, although typically one would investigate the aerodynamics at the resonant frequencies of the structural model (as the system is weakly coupled), which are readily available.

Of course there is an associated loss of generality and accuracy in using a linearized method to approximate finite motion as we do here. This effect will be examined for the particular case of unstructured finite volume codes. The assumption of linearity means that the results are only valid for small perturbations of the geometry, and any non-linear effects of the flow that cause, for example, shifts in frequency or harmonic modes, will not be modeled. Nonetheless, there is a growing body of evidence that indicates that linear Euler and Navier-Stokes calculations are adequate for a wide range of applications,[12,20,22,28] although up until now predominantly in problems in turbo machinery.[5,15–17,21] We add to this evidence in this paper.

In algorithmic terms we contribute the result that an entire frequency domain calculation may cost only the equivalent of 3 RANS calculations. This is an substantial gain over full unsteady analysis, which might require the equivalent of $50 - 100$ steady flow computations, when the requirements of deformation of the mesh at each time-step, damping of initial transient motion and post-processing are taken into account.

The following Section describes the Fourier transform procedure applied to a general PDE discretized in space. We consider implementational issues on the example of an unstructured finite volume compressible RANS code, the DLR TAU-code, in particular with reference to linearization and linear solution methods. The LFD method is then verfied against URANS results, computed with the full non-linear version of the same solver. We therefore expect to see identical results in the limit of small perturbations. The accuracy of the linearization is then examined for a variety of test cases: a subsonic, inviscid flow around a NACA 0012 aerofoil and for three viscous cases, the NACA 64A010 aerofoil, the AGARD LANN wing and the DLR-F12. In all these cases the accuracy of the LFD solver is demonstrated, and we can conclude that the approach is suitable for the aeroelastic analysis of transonic airplane flows.

2 THE LINEARIZED FREQUENCY DOMAIN SOLVER

2.1 Fourier Transformation of the Discretized System

The unsteady governing equations of a fluid, discretized in space with an arbitrary method be written in a *semi-discrete form*:

$$\frac{\mathrm{d}u}{\mathrm{d}t} + R(u, x, \dot{x}) = 0, \tag{1}$$

where R is termed the residual, and is a function of the flow solution u, the grid x and the grid velocities $\dot{x}$. The movement of the grid, characterized by $x(t)$ is taken to be known, and (1) must be solved for $u(t)$. In the following discussion the equations discretized by R, and the particular form of the discretization is not important. In later sections however we will apply this general theory to finite volume discretizations on unstructured grids of the the compressible Euler equations (inviscid) and the compressible Navier-Stokes equations.
By assuming the unsteady motion has a small amplitude it is possible to separate the unsteady terms above in terms of a steady mean state and a small perturbation:

$$\begin{aligned} u(t) &= \bar{u} + \tilde{u}(t), \qquad \|\tilde{u}\| \ll \|\bar{u}\| \\ x(t) &= \bar{x} + \tilde{x}(t), \qquad \|\tilde{x}\| \ll \|\bar{x}\| \end{aligned}$$

whereby

$$\dot{x}(t) = \dot{\tilde{x}}(t)$$

and where $\bar{u}$ indicates the mean state and $\tilde{u}$ the perturbation. Substituting this into (1) and linearizing about the steady mean state results in

$$\frac{\mathrm{d}\tilde{u}}{\mathrm{d}t} + \left.\frac{\partial R}{\partial u}\right|_{\bar{u},\bar{x}} \tilde{u} + \left.\frac{\partial R}{\partial x}\right|_{\bar{u},\bar{x}} \tilde{x} + \left.\frac{\partial R}{\partial \dot{x}}\right|_{\bar{u},\bar{x}} \dot{\tilde{x}} = 0, \tag{2}$$

which is a time-dependent linear equation for the flow perturbation.
Additionally, the motion and the flow solution are assumed to be periodic, so that it can be written as a Fourier series

$$x(t) = \bar{x} + \tilde{x}(t) = \bar{x} + \sum_k \mathcal{R}(\hat{x}_k e^{ik\omega t}) \tag{3}$$

$$u(t) = \bar{u} + \tilde{u}(t) = \bar{u} + \sum_k \mathcal{R}(\hat{u}_k e^{ik\omega t}) \tag{4}$$

where $\hat{x}_k$ and $\hat{u}_k$ are complex Fourier coefficients of the motion and ω is the base frequency with k the mode.
Neglecting the real-part operator and substituting into (2) we obtain an equation for each mode k

$$\left\{ ik\omega I + \frac{\partial R}{\partial u} \right\} \hat{u}_k = -\frac{\partial R}{\partial x}\hat{x}_k - ik\omega \frac{\partial R}{\partial \dot{x}}\hat{x}_k, \tag{5}$$

which are decoupled due to linearity. Therefore given a small periodic deformation of the grid represented by $\hat{x}_k$, the Fourier coefficient of the fluid motion may be found by solving (5) individually for each mode. The accuracy of the result will depend on the degree to which the dual assumptions of small perturbations and linearity are satisfied.

From this point we assume that we are interested only in perturbations of the system that are harmonic in time. Therefore we take the convention that $k = 1$, and we will only need to solve (5) once. Hence an real time-dependent non-linear system has been reduced to a single complex linear system using the assumptions of small perturbations and periodicity. In the following we discuss the solution of this linear system.

2.2 Implementation of the Linearized Equations

Instead of solving the complex system (5) it is split into two coupled real systems by taking real and imaginary parts. This results in:

$$-\omega\hat{u}_{\mathrm{Im}} + \frac{\partial R}{\partial u}\hat{u}_{\mathrm{Re}} = -\frac{\partial R}{\partial x}\hat{x}_{\mathrm{Re}} + \omega\frac{\partial R}{\partial \dot{x}}\hat{x}_{\mathrm{Im}}, \tag{6}$$

$$\omega\hat{u}_{\mathrm{Re}} + \frac{\partial R}{\partial u}\hat{u}_{\mathrm{Im}} = -\frac{\partial R}{\partial x}\hat{x}_{\mathrm{Im}} - \omega\frac{\partial R}{\partial \dot{x}}\hat{x}_{\mathrm{Re}}, \tag{7}$$

where $\hat{u} = \hat{u}_{\mathrm{Re}} + i\hat{u}_{\mathrm{Im}}$ etc. This may then be written in explicitly as a single linear system,

$$Ax = b, \tag{8}$$

where the system matrix is

$$A = \begin{bmatrix} \frac{\partial R}{\partial u} & -\omega I \\ \omega I & \frac{\partial R}{\partial u} \end{bmatrix}, \tag{9}$$

and where I is the identity matrix of the same dimensions as the Jacobian.
The Jacobian $\partial R/\partial u$ has been obtained previously in the context of the discrete adjoint method by hand-differentiating the code and is available in the *TAU* solver.[9] Considerable attention has been given to ensure that the evaluation of the Jacobian and matrix-vector products involving the Jacobian are efficient in terms of memory and time. In particular the (time-domain) linearized code requires no more than four times the memory requirements of the non-linear code, and a single residual evaluation is 60%-80% the cost of the non-linear residual evaluation in terms of CPU time.[8] The frequency domain residual however requires two products of a vector with the Jacobian, and hence a single evaluation is approximately 120%-140% the cost of a non-linear residual on the same case.

Finally the right-hand side terms $\partial R/\partial x$ and $\partial R/\partial \dot{x}$ are needed, which are evaluated using central finite differences:

$$\frac{\partial R}{\partial x}\hat{x} \approx \frac{R(\bar{u}, \bar{x} + \epsilon\hat{x}, 0) - R(\bar{u}, \bar{x} - \epsilon\hat{x}, 0)}{2\epsilon}, \tag{10}$$

$$\frac{\partial R}{\partial \dot{x}}\hat{x} \approx \frac{R(\bar{u}, \bar{x}, \epsilon\hat{x}) - R(\bar{u}, \bar{x}, -\epsilon\hat{x})}{2\epsilon}, \tag{11}$$

where $\epsilon > 0$ is the finite difference step size chosen small enough to avoid errors due to higher-order terms, while large enough to avoid errors arising from the limited accuracy of the residual. In particular for Navier-Stokes calculations it can be difficult to find a suitable ϵ, and a parameter study must be performed to obtain a reliable value. This is an expensive process, and it would be desirable to have these partial derivatives available in a hand-differentiated, or automatically differentiated (AD)[14] form.

2.3 Iterative Solution Method

Usually the solution method is the most critical algorithm for solver efficiency – as such significant effort has been expended in developing solution methods for the steady non-linear problem. Given the close relationship of the linear and steady non-linear problem, it is reasonable to expect a correspondence in performance to a method applied to the two systems. Specifically, in the context of adjoint methods, it has been shown that fixed-point iterations developed for the non-linear system (for example Runge-Kutta with multigrid), can be applied to the linear system in such a manner as to *guarantee* the convergence of the linear iteration *given* the asymptotic convergence of the non-linear iteration.[7,9] Furthermore it can be shown that the asymptotic rate of convergence of the two cases must be identical.

However, such a precise statement is not possible in the case of the LFD solver, as (5) is not a simple linearization of the non-linear equation, but involves additional ωI terms on the diagonal. Nonetheless the system is predominantly characterized by the Jacobian, and the fixed-point iterations for the non-linear system may therefore be appropriate. In the case of implicit methods[7] the implicit system matrix can be relatively easily modified to admit the additional ω term, after which the performance of the modified and original explicit schemes might be expected to be comparable. This has been performed for the LU-SGS scheme in *TAU*.

Demonstration of the similar convergence behavior of the non-linear and LFD versions of multigrid damped LU-SGS is shown in Figure 1. A NACA0012 aerofoil at Mach 0.4 and an angle-of-attack of 4° undergoes pitching oscillation with an amplitude of 1° and several reduced frequencies. First the steady flow is computed and after 500 iterations the resulting solution is taken as the steady mean flow for the frequency domain calculations. All calculations use the same CFL number and multigrid cycle. On the left of Figure 1 the convergence for a reduced frequency of 0.1 is compared with non-linear convergence. As is immediately apparent the residuals drop at the similar rates, and the force coefficients also show similar rates of convergence. On the right-hand side the independence of the convergence for a wide range of frequencies is demonstrated.

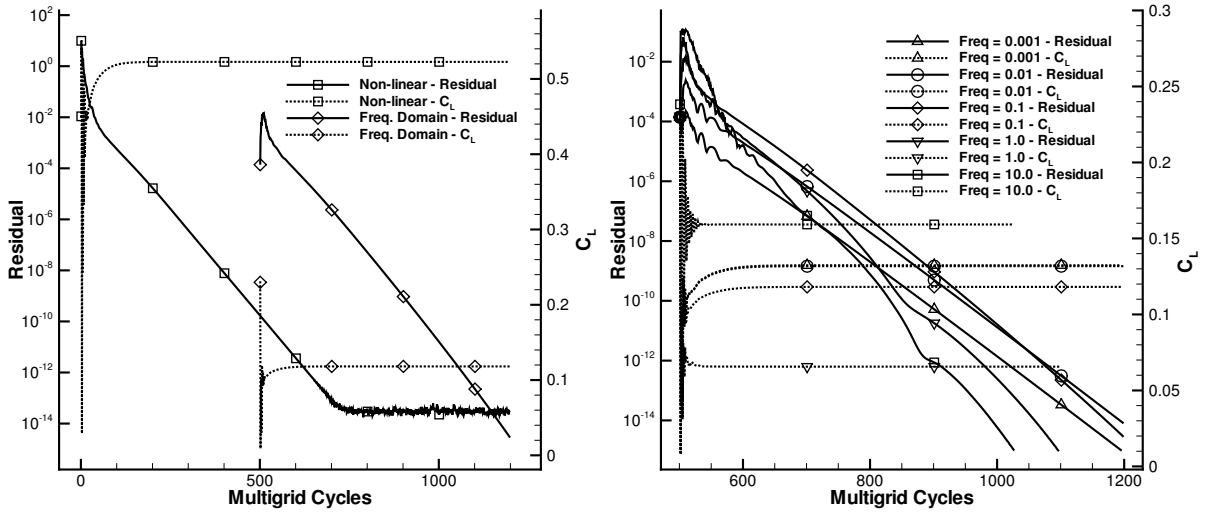

Figure 1: Convergence of the non-linear solver and the frequency domain solver restarted from a mean flow field achieved after 500 iterations. The convergence of C_L and the amplitude of the C_L oscillation respectively are also shown. On the right convergence for a range of reduced frequencies is shown.

As a consequence, the number of iterations required for the frequency domain code should be of the same order as that of the non-linear code, and hence the total CPU time requirement is only about 20%-60% greater than the corresponding stationary flow solution.
For viscous and turbulent flows the same idea applies in principle , but in practice it

is often necessary to use some additional stabilization technique, such as the Recursive Projection Method (RPM)[13,25] or other Krylov methods.[4] This is due to the fact that in the majority of cases some part of the solution fails to converge asymptotically in the non-linear problem, often seen as stalling in the residual convergence. This is not a serious issue provided the non-linear residual is small enough – however since the non-linear iteration is asymptotically unstable, it can not be expected that the iteration on the linear system converges. In this work we apply the well-known Generalized Minimum Residual (GMRes) Krylov method in a restarted variant.[23,24] The size of the restart vector was 20, which was sufficient to stabilize the iteration in all the cases examined here.

2.4 Simulation Process

All steps involved in the computation of the frequency response are described to give a clear overview of the method.

1. Compute a steady flow solution $\bar{u}$ at the mean state $\bar{x}$, by solving the non-linear system $R(\bar{u}, \bar{x}) = 0$.

2. Compute the right-hand side terms in (5), using the state $\bar{u}$, $\bar{x}$. If this is performed with finite differences it will involve application of (10) and (11), which involve several deformations of the computational mesh $\bar{x} \rightarrow \bar{x} \pm \epsilon\hat{x}$.

3. Solve the linear system (5) to obtain $\hat{u}$, the Fourier coefficients for the solver degrees of freedom (DoFs).

4. Calculate the Fourier coefficients of the quantities of interest. These are seldom the DoFs themselves – for example in our context the DoFs are conservative variables, but the pressure is the aerodynamically interesting quantity. In this case use $\hat{p} = \frac{\partial p}{\partial u}\hat{u}$, and similarly for forces (C_L, etc.) and moments (C_{My}, etc.)

3 NUMERICAL METHOD

The unsteady DLR *TAU*-Code[10,26] solves the compressible, three-dimensional Reynolds-Averaged Navier-Stokes equations using a finite volume formulation. *TAU* is based on a hybrid unstructured-grid approach, which makes use of the advantages of semi-structured prismatic grids in the viscous shear layers near walls, and the flexibility in grid generation offered by tetrahedral grids in the surrounding flow volume. A dual-grid approach is used in order to make the flow solver independent from the cell types used in the initial grid. The *TAU*-Code consists of several different modules, including:

- The Preprocessor module, which uses the information from the initial grid to create a dual-grid and secondly coarser grids for multi-grid.

- The Solver module, which performs the flow calculations on the dual-grid.
- The Linear Solver module, which solves the complex valued linear system of equations subsequently on the same dual-grid.
- The Deformation module, which propagates the deformation of surface grid points to the surrounding volume grid.
- The Postprocessing module, which is used to convert result-files to formats usable by popular visualization tools.

The mentioned modules are available through *Python*-scripting. This approach makes them available inside the main *TAU* workflow by minimizing file I-O, easing parallel set up and easily simplifies looping processes.
Turbulent flow computations were performed with the one equation turbulence model established by Spalart-Allmaras.[27] The linear solver underlies some restrictions in the completeness of a fully hand-differentiated code. The viscous effects are kept constant for the Matrix $\frac{\partial R}{\partial u}$ and turbulent effects are neglected completely.

4 VALIDATION RESULTS

Four representative test cases were chosen to show the capability of the linearized frequency domain (LFD) solver and validity in comparison to fully unsteady (URANS) computations. The first case is a NACA 0012 aerofoil in subsonic, inviscid flow undergoing heave motion to point out the range of applicability between linear and non-linear computation. Then a transonic flow around a NACA64A010 aerofoil undergoing periodic pitching movement, generally referred as CT8 case found in AGARD-R-702,[6] will present results from the LFD, unsteady computation and experimental data. Finally two three-dimensional cases are examined: the AGARD LANN wing with a complex shock structure, referred as CT5, and the F12 with a more complex geometry, including wing, horizontal tail plane and fuselage.
In context of dimensionless quantities the reduced frequency k is applied as similarity parameter for the unsteadiness of the flow field. The reduced frequency k is defined as:

$$k = \frac{\omega\, l_{ref}}{U_\infty} = \frac{2\pi f\, l_{ref}}{U_\infty} \tag{12}$$

with the angular velocity ω, the free-stream velocity U_∞, frequency f and a reference length l_{ref}. The harmonic motion imposed is described by

$$\text{pitch: } \alpha(\tau) = \bar{\alpha} + \tilde{\alpha} \cdot sin(k \cdot \tau) \tag{13}$$

$$\text{heave: } h(\tau) = \bar{h} + \tilde{h} \cdot sin(k \cdot \tau) \tag{14}$$

$$\text{dimensionless time: } \tau = \frac{U_\infty t}{l_{ref}}.$$

Throughout the validation section different reduced frequencies k, mean and incident amplitude angles are applied.

Another usual description in aeroelastic means is the real and imaginary part of the surface pressure distribution C_p. The aerodynamic description of C_p is :

$$C_p = \frac{p - p_\infty}{\frac{1}{2}\rho_\infty U_\infty} = \bar{C}_p + C^*_{p-real}\sin(k\tau) + C^*_{p-imag}\cos(k\tau) \tag{15}$$

with ∞ values at free-stream conditions and p as the static pressure at measurement. The real and imaginary part of C_p are normalized with the amplitude of the forcing motion.

$$C^*_{p-real} = \frac{C_{p-real} \cdot 180^o}{\tilde{\alpha} \cdot \pi} \quad \text{and} \quad C^*_{p-imag} = \frac{C_{p-imag} \cdot 180^o}{\tilde{\alpha} \cdot \pi} \tag{16}$$

to represent the pressure distribution independent of imposed incident amplitude $\tilde{\alpha}$ or $\tilde{h}$. Table 1 gives an overview of the relation between frequency f and reduced frequency k

Test case	k [1]	Mach number [1]	$\tilde{\alpha}$ [°] or $\tilde{h}$[m]	f [Hz]	l_{ref}[m]
NACA 0012-heave	1e-5	0.5	0.1	0.00027	1
NACA 0012-heave	0.1	0.5	0.1	2.7	1
NACA 0012-heave	1	0.5	0.1	27	1
NACA 64A010-pitch	0.2	0.8	0.5	4.3	1
AGARD LANN-pitch	0.204	0.82	0.25	8.82	1
DLR F12-pitch	0.068	0.205	4.52	3	0.253

Table 1: Distinct motion data for the test cases chosen.

with Mach number in use for the test cases in that section. A real aircraft has a typical lowest, elastic, structural frequency about 1 Hertz.

4.1 NACA0012 Heave Oscillations - inviscid subsonic flow

The NACA0012 is a symmetrical aerofoil that performs a heave oscillation. The flow conditions are a subsonic free-stream Mach number of 0.5 with an angle of attack $\bar{\alpha}$ of 0.16° and an incidence amplitude $\tilde{\alpha}$ of 0.1° with a reduced frequency range from 10^{-5} up to 10. A fine grid with about 17.000 mesh points was chosen to capture flow physics at higher frequencies.
Further it should be mentioned that the number of time-steps per period and inner pseudo time multigrid cycles for the dual time stepping varied over the frequencies. Lower frequencies needed a much higher resolution per period while the inner pseudo time steps increased with higher frequencies. To provide the appropriate accuracy for the solutions a convergence criterion for the inner cycles was set to the global lift and drag coefficients,

for changing relatively less than 10^{-6} the inner pseudo time-stepping had finished. The steady state solutions and the LFD convergence have been performed until machine accuracy, while the density residual was used for the flow simulation and the first entry of real and imaginary solution vector for the LFD, respectively.

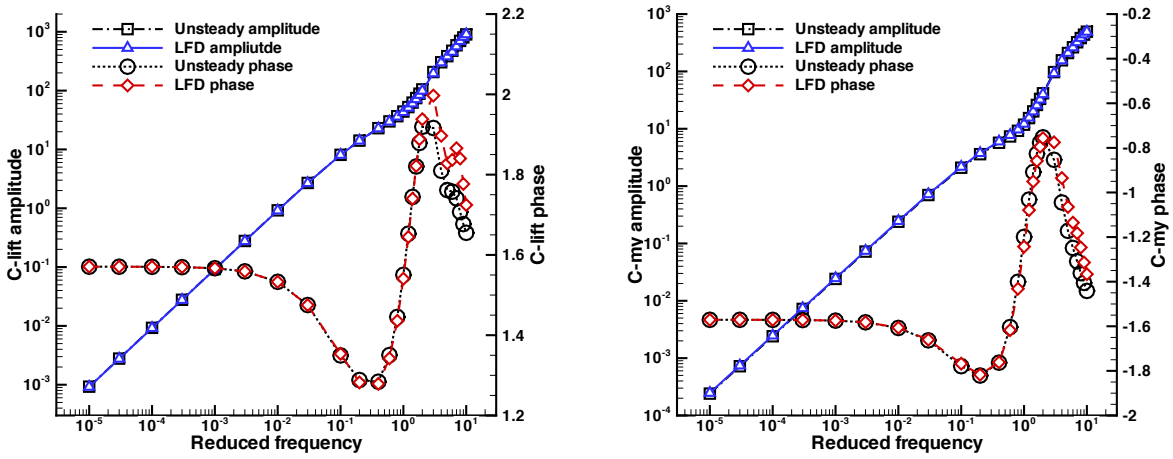

(a) Lift

(b) Pitching moment

Figure 2: NACA 0012 undergoing harmonic heave movement for a incidence amplitude $\tilde{h}$ of 0.1m over a wide range of reduced frequencies showing the amplitude and phase behavior for lift and pitching moment for the LFD in comparison to unsteady simulations.

Figure 2 is a compact presentation of the frequency response of lift (a) C_L and pitching moment (b) C_{My} in amplitude and phase from the LFD in comparison to unsteady simulations. Analogous to the pressure coefficient, the amplitude of the lift and moment coefficient is normalized with the amplitude of the forcing motion.
Because the profile performs a heaving motion, the effective pitching amplitude, which governs the flow physics, is $\tilde{h} \cdot k$ and so the amplitude is linearly dependent on the reduced frequency. For lower reduced frequencies ($k \leq 1$) the amplitudes of lift and pitching moment are linear with respect to the frequency and the LFD and URANS results agree very well. For the limit of $k \to 0$ the lift and moment amplitudes will approach zero too, and the phase is 90° for the lift and -90° for the pitching moment. With increasing reduced frequency the effective amplitude of the angle of attack increases as well. Non-linear effects, here a transonic region that appears and disappears over one period (see Figure 3), are occurring and cannot be captured by the time-linearized solver anymore.

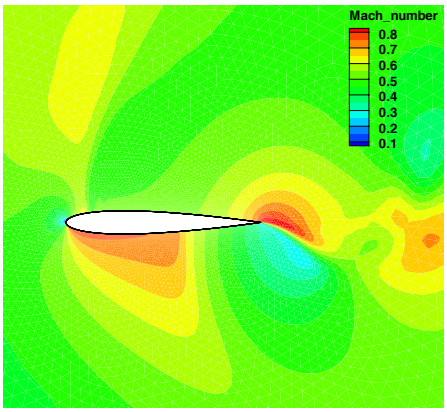

(a) $\frac{1}{4}$ period

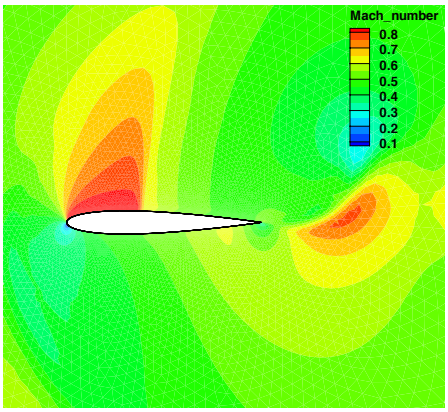

(b) $\frac{1}{2}$ period

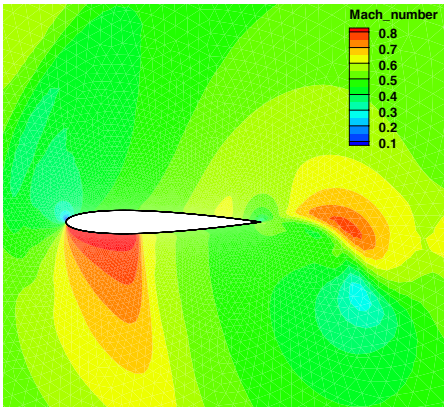

(c) $\frac{3}{4}$ period

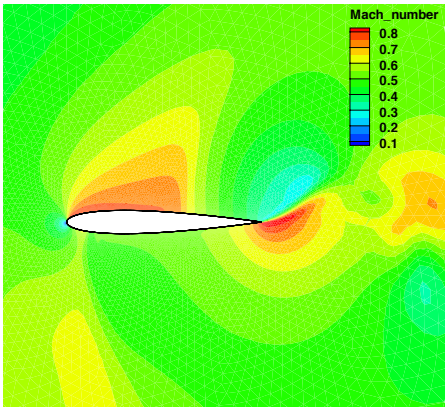

(d) 1 period

Figure 3: Mach number contours at four stages of a period for NACA 0012 undergoing harmonic heave movement for a incidence amplitude $\tilde{\alpha}$ of 0.1°and reduced frequency $k = 2$.

4.2 NACA64A010 Pitch Oscillations - transonic viscous

The CT8 case from AGARD-R-702[6] is a transonic case with a freestream Mach number of 0.8, a Reynolds number of 12.5 million and an angle of attack of zero degrees. The pitching motion is performed at a x-axis of 25% from the chord length and the incidence amplitude will be $\tilde{\alpha} = 0.5°$. The computational grid, left Figure 4, contains 10727 points with 11630 quadrilaterals for the boundary layer resolution and 4800 triangles for the remaining flow field and the flow simulation was performed with a LUSGS semi-implicit time stepping scheme and a 4w multigrid cycle. One period of the URANS simulation is resolved with 150 steps per period and the same convergence criterion for the inner multigrid cycles was set as for the heave case at 4.1.

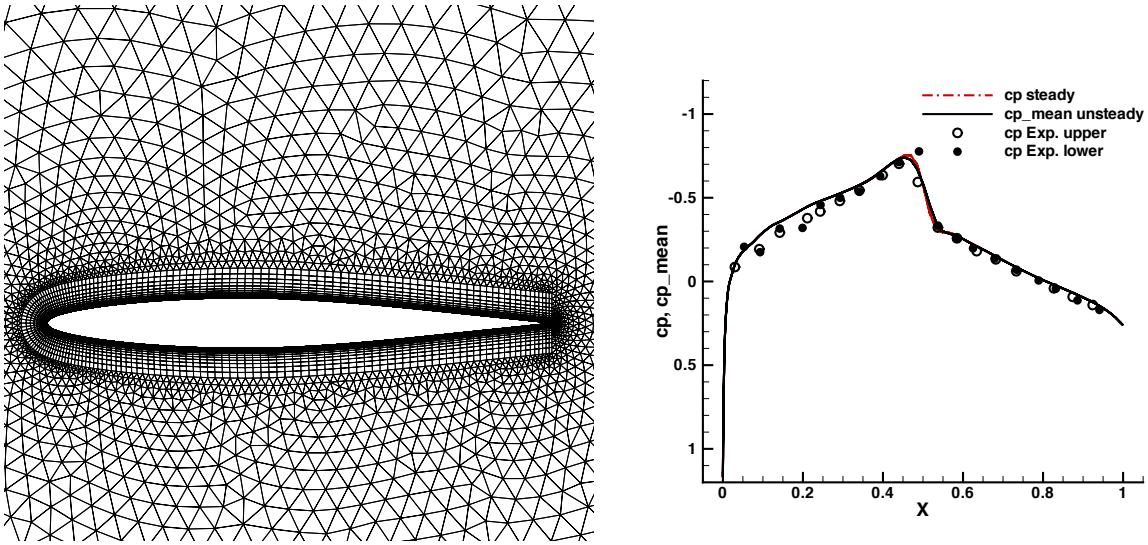

(a) Mesh (b) C_p

Figure 4: Computational grid (left) and surface pressure distribution (right) for Ma=0.8, Re=12.5 million and $\bar{\alpha} = 0.0°$from the steady state, unsteady mean value and experimental data.

Evaluating the prediction quality of the LFD, the pressure distribution C_p on the aerofoil contour are shown. The steady state and mean pressure coefficient, Figure 4 (b), compared with the experimental data shows small deviations in the pre-shock region but good agreement in the post-shock region. The pressure gradient in the shock region of the LFD and the steady state differs from the mean value of the URANS simulation due to nonlinear effects.
Real and imaginary parts of the first harmonic pressure C_p, Figure 5, reveals an excellent agreement between the LFD compared to unsteady simulation, except for the different peaks in the shock regions were the real part overestimates and the imaginary part underestimates the peak. So there is an error in phase due to a non-harmonic motion of

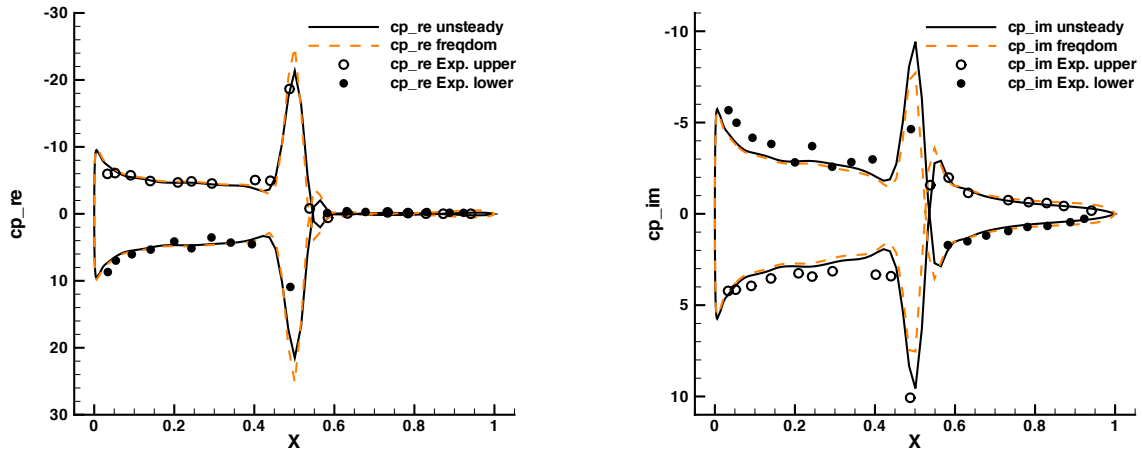

(a) C_p real (b) C_p imaginary

Figure 5: Comparison of real and imaginary part of surface pressure coefficient distribution for NACA64A010 aerofoil with Ma=0.8, Re=12.5 million, $\bar{\alpha}$=0.0°, $\hat{\alpha}$=0.5°and k=0.2 .

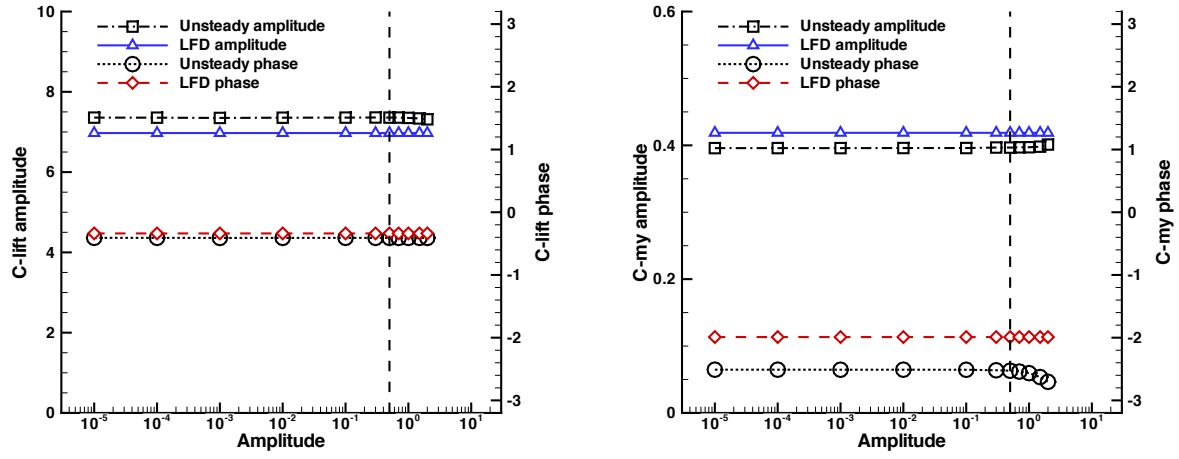

(a) Lift (b) Pitching moment

Figure 6: NACA64A010 aerofoil undergoing harmonic pitch oscillation for a range of incidence amplitudes at $k = 0.2$ for the lift and pitching moment amplitudes and phase.

the shock. The unsteady simulation is able to resolve at the shock with higher harmonics while the LFD resolves the region first order accurate which can be seen in a phase shift deviation. The shock range around x=0.5 is nearly the same for both simulations

and serves as an indication that the amplitudes of the global forces and moments will be represented accordingly as for the unsteady simulation.

Investigations were conducted to present the influence of increasing incidence amplitudes by keeping the reduced frequency constant. Starting with $\tilde{\alpha}$ of 10^{-5} and increasing up to a value of 2, Figure 6(a) and (b), the amplitudes for lift and pitching moment show a constant distribution for the LFD which follows from the behavior of the linearization. The unsteady distribution does not vary up to about $\tilde{\alpha}$ of 1.5° but deviates at higher $\tilde{\alpha}$ because of non-linear effects in the flow seen in Figure 6(b) for the amplitude and phase of the pitching moment. In addition there is not seen any evidence for amplitude dependency using finite differences for creating vector b (10) for the linear system.

Up to know it is not clear why the phase of the pitching moment is approximately 25° off from the unsteady results, but one extended survey has to estimate for the influences of the linearized viscous terms and the integration of global forces and moments. All other distributions are within expected ranges especially lift amplitudes and phases can be predicted properly up to $\tilde{\alpha}$ values of 2 .

4.3 LANN Wing Pitch Oscillations - transonic viscous

The AGARD LANN wing[29] is a trapezoidal 3D wing, typical for transport aircraft flying in transonic flow regions. The ratio between halfspan width and root chord length is about 2.77. The wing performs a pitching motion around a x-axis of $x = 0.62$ with a freestream Mach number of 0.82, a Reynolds number of 7.3 mill., a mean angle of attack of $\bar{\alpha} = 0.6$, an amplitude of 0.25° and a reduced frequency of $k = 0.204$. The test case

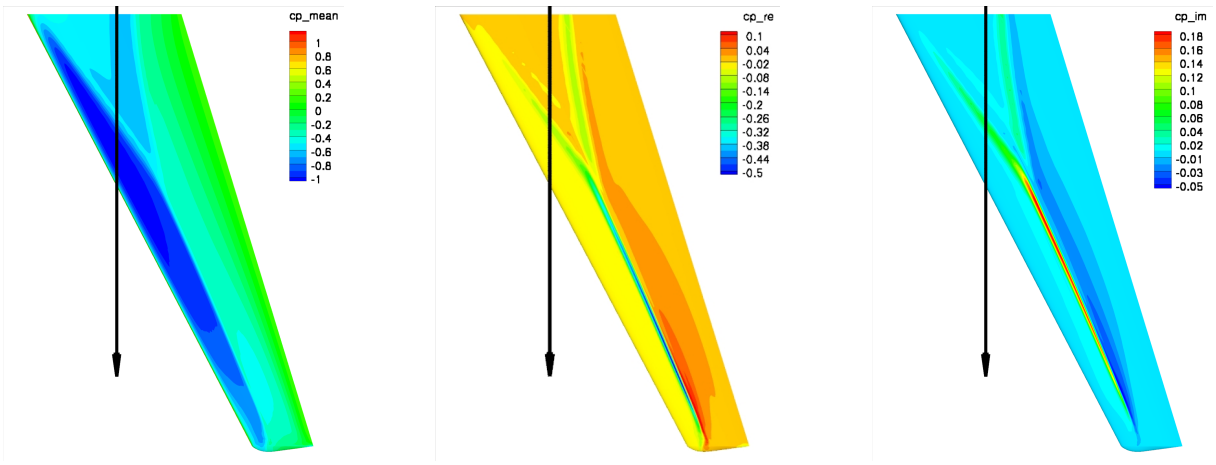

(a) C_p^{mean} (b) C_p^{real} (c) C_p^{imag}

Figure 7: C_p contour on the upper side of the AGARD LANN wing - case CT5

provides a more complex shock system, a typical λ shock system on upper side of wing, see Figure 7 (a).

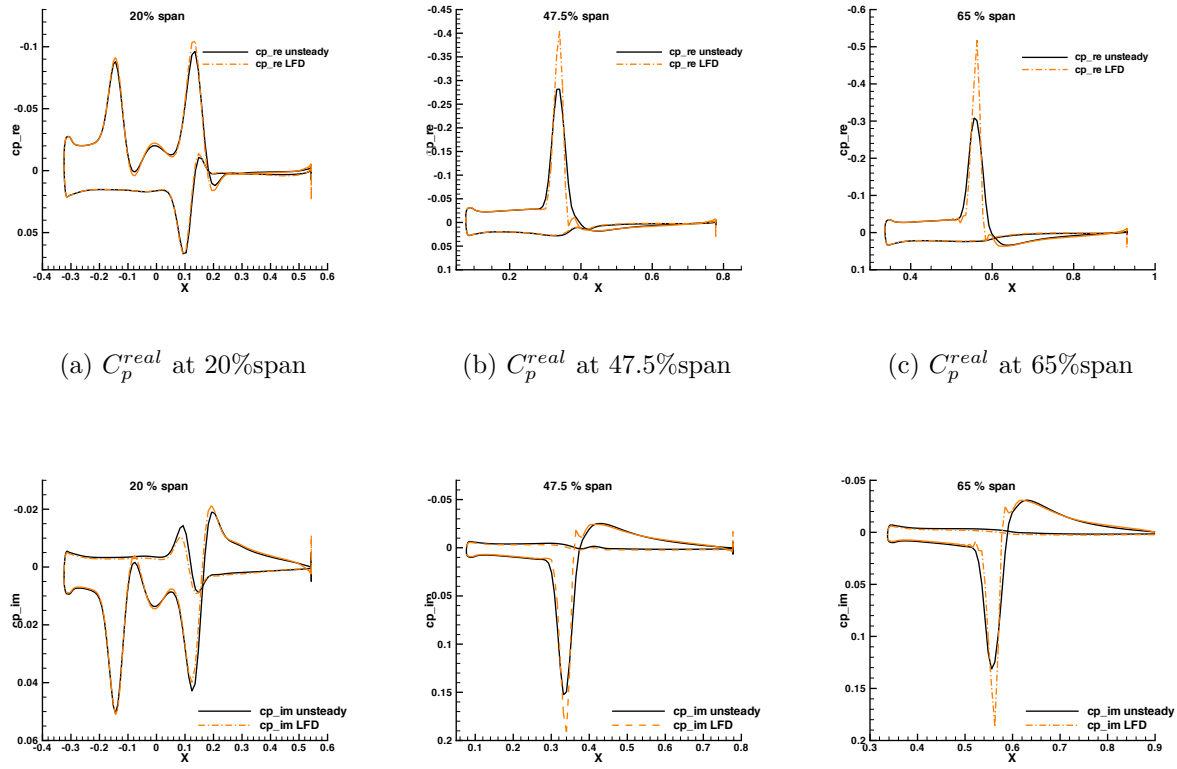

(a) C_p^{real} at 20%span (b) C_p^{real} at 47.5%span (c) C_p^{real} at 65%span

(d) C_p^{imag} at 20%span (e) C_p^{imag} at 47.5%span (f) C_p^{imag} at 65%span

Figure 8: Real and imaginary parts of the surface pressure distribution at distinct cut planes from the LANN Wing.

In Figure Figure 7 (b) and (c) the surface pressure distribution is presented in real and imaginary part as contour plot and in Figure 8 the local C_p distribution at three spanwise positions of the LFD is compared to the non-linear time domain solver.
Overall, the LFD and URANS results agree very well except for some differences in the shock regions. In the inner region of the wing the angular shock is well captured, but the normal shock behind has a small phase error, see Figure 8 (a) and (d). There are also some differences in the imaginary part at the weak shock at the lower side of the wing. In the outer regions, see Figure 8 (b),(c),(e) and (f), of the wing the real and imaginary part of C_p is overshot in the strong shock region. Here higher harmonics can not be neglected to describe the shock motion, but a time linear solver can only consider the first harmonic and so it overshoots the amplitude and the phase is different, too.

4.4 DLR F12 Pitching Oscillations - transonic viscous

The DLR-F12 wind tunnel model is a generic transport aircraft configuration, designed for dynamic wind tunnel tests in the DNW-NWB. It has a span of $b = 2.036\,m$, a reference chord of $l_\mu = 0,253\,m$ and a fuselage length of $l = 2.238\,m$. It is of modular design, and made of carbon fiber sandwich construction, having a weight of approximately 12 kgs. and permits the measurement of steady and unsteady forces, moments and pressure distributions. In order to assess the accuracy of the experimental and numerical methods used for the prediction of the dynamic derivatives, systematic investigations have been performed in several wind tunnel tests using this model.

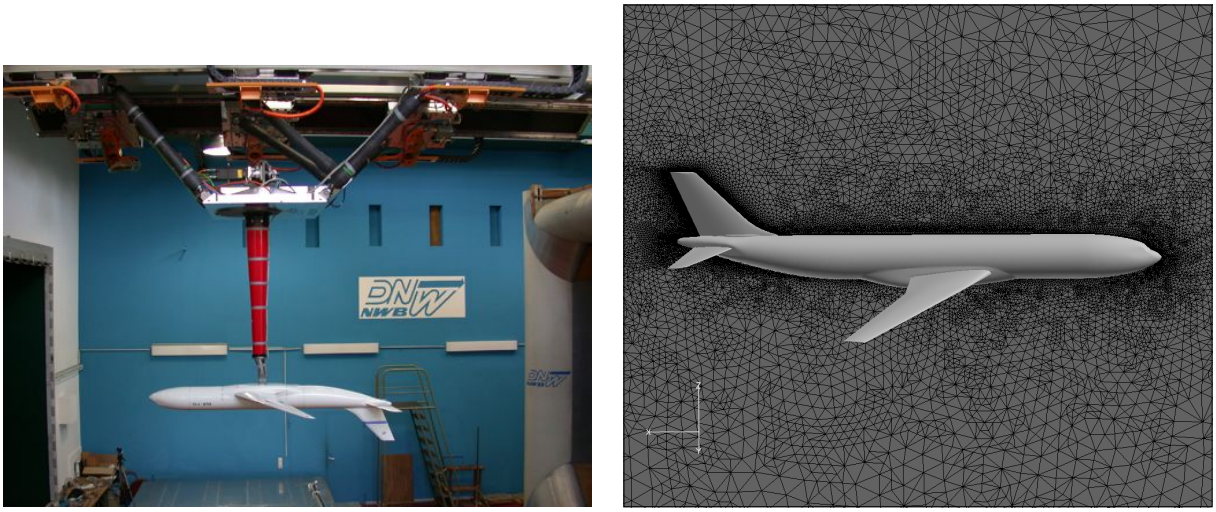

(a) Windtunnel model

(b) Computational grid

Figure 9: Testing facilities of the DLR F12 model (left) in the NWB windtunnel at Braunschweig and right the computational grid for the unsteady and LFD simulations.

The model was mounted with a ventral sting onto NWB's Model Positioning Mechanism (MPM). The MPM can be described as a 6-Degree-of-Freedom (DOF) parallel kinematics system incorporating six struts of constant length whose joints at the wind tunnel fixed side connect to six electric linear motors. The MPM has been in operation since 2004 and is located above the test section. The MPM with the F12 model installed is shown in Figure 9(a). More details concerning the MPM can be found in Ref.[2,18] The computational grid, Figure 9(b), contains 9.6 million points with 12.73 mill. prisms for the boundary layer resolution and 17.62 mill. tetrahedra for the remaining flow field.

Comparing additionally the surface pressure distributions two representative spanwise cuts were chosen on the wing at 45% span and on the horizontal tail plane (HTP) at 46% span. Mean C_p, especially at the wing section in Figure 10 (a) and slightly smoother for

the HTP in (d) displays a highly visible unsteadiness in the nose region. Irrespectively of the low frequency of 3 Hertz, the incidence amplitude of 4.5° imposes a strong movement of the suction and pressure region. Furthermore the Figure 10 (b) and (e) for the real part of C_p show the behavior of spurious oscillations over the HTP, especially seen at the trailing edge.

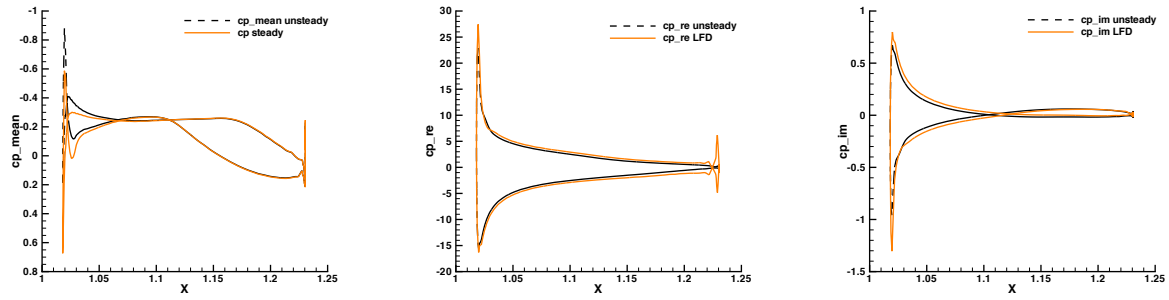

(a) Wing: C_p^{mean} at 45% span

(b) C_p^{real} at 45% span

(c) C_p^{imag} at 45% span

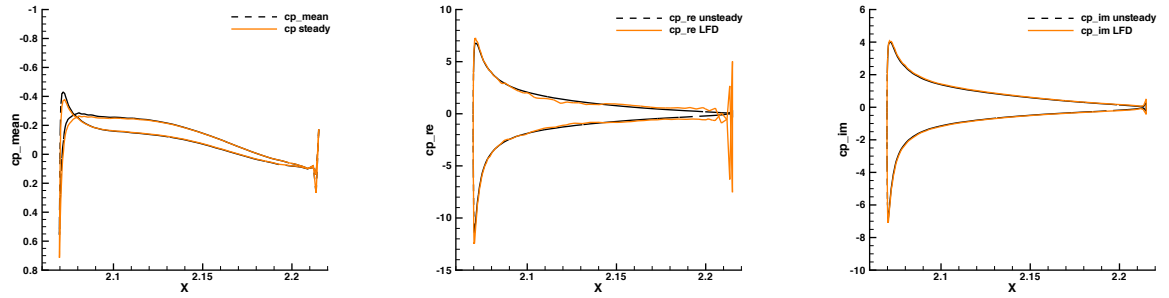

(d) HTP:C_p^{mean} at 46% span

(e) C_p^{real} at 46% span

(f) C_p^{imag} at 46% span

Figure 10: Real and Imaginary part of surface pressure distribution of the wing and at the HTP.

This phenomenon is introduced by the evaluation of the right hand side vector b in (10) with finite differences. The appropriate ϵ is difficult to find for this test case because the pitching axis is near the main wing and the HTP is far off. Either the ϵ is too small, then the generated values for the wing are only random noise and the HTP will be modeled properly, or vice versa finding the proper ϵ for the wing will lead to oscillations for the HTP. For this test case five different ϵ were tested, which are computed in less than a minute before actually starting the LFD and visualizing the vector b (10) for oscillations. Up to now, searching for a reliable finite differences ϵ is a long term engineering process

but can be reduced by having a differentiated version to evaluate the right hand side vector b in the near future.

For the imaginary C_p of the wing in Figure 10 (c) the LFD shows a slightly expanded distribution in comparison to the URANS which is caused by the strong unsteadiness in the nose region which can not be resolved from the linear solver but in general there is a good agreement with the URANS simulation.

4.5 Computational Effort

One of the key-issues of the LFD solver is the computational performance in comparison to unsteady time accurate simulations and during the validation process time measurements were made to emphasize the possible time reduction for Euler and Navier-Stokes computations. Table 2 presents the time efficiency for the test cases and additionally the time used for unsteady, together with the number of periods computed, and LFD is shown with the number of processors for parallel applications. The first two entries for the NACA 0012 Euler simulations exhibit an improved time reduction factor when switching from subsonic into transonic flow regimes. However, the number of periods and inner pseudo time steps performed can drastically increase the unsteady time effort but usually a reduction factor of about 15 to 20 was observed for Euler test cases.

Test case	unsteady	LFD	# proc.	time reduction factor
NACA 0012 Euler Ma=0.5	5146 s (p=3)	441 s	1	≈ 11.5
NACA 0012 Euler Ma=0.755	13860 s (p=5)	814 s	1	≈ 17
NACA 64A010 RANS Ma=0.8	7100 s (p=5)	580 s	1	≈ 12.2
LANN Wing RANS Ma=0.82	833 h (p=3)	58 h	8	≈ 14.4
DLR F12 Ma=0.205	4128 h (p=2)	256 h	32	≈ 16.1

Table 2: Computational effort in seconds (s) and hours (h) and time reduction factors for distinct test-cases were p is the number of periods simulated for URANS.

The last three viscous cases in Table 2 have a generally lower reduction factor of around 10 to 15. In parallel, the LFD's communication is increased dramatically by solving the double solution vector and for viscous cases the convergence rate does not behave similarly to the steady simulation anymore. In fact, the residual drops much less and often flattens after a certain amount of iterations.

5 CONCLUSIONS

An efficient linear solver for predicting aerodynamic stability data has been shown for inviscid as well as for viscous flows which can serve as a powerful alternative tool for aeroelastic applications. The validity of this approach was demonstrated for simple test cases emphasizing the accuracy for a wide range of frequencies and incidence amplitudes.

Additionally a test case with a complex shock system and a well-investigated windtunnel model was used to point out the experience gained through the simulation with the LFD solver for such a realistic use.

Overall good agreement in the results between the LFD and the time accurate flow solver as well as experimental data could be presented. Savings in computational time up to an order of magnitude are shown for all test cases. Future work will focus on the completeness in the linearization procedure for viscous terms and turbulent equations to investigate their influence on the results and to consider more complex flows with e.g. shock induced separations. Furthermore, the development of an hand-differentiated mesh sensitivity tool for generating the right hand side vector b independently of a finite differences ϵ is a main concern to establish the linearized frequency domain solver for complex configurations.

ACKNOWLEDGMENTS

The authors wishes to thank Ralph Voss from the Institute of Aeroelasticity in Göttingen for his continuous support while creating this manuscript with many helpful advisories on unsteady flow physics.

REFERENCES

[1] E. Albano and W. P. Rodden. A doublet lattice method for calculating lift distributions on oscillating surfaces in subsonic flows. *AIAA Journal*, **7**(**2**):279–285, February 1969.

[2] A. Bergmann, A. R. Hübner, and T. Löser. Experimental and numerical research on the aerodynamics of unsteady moving aircraft. *Progress in Aerospace Sciences*, **4**4:121–137, 2008.

[3] G. Brendes and R. Voss. Transonic flutter calculations for a low wing transport aircraft using the transonic doublet lattice method. In *IFASD*, Madrid/Spain, June 5-7 2001. International Forum on Aeroelasticity and Structural Dynamics.

[4] M. Campobasso and M. Giles. Stabilization of a linear flow solver for turbomachinery aeroelasticity by means of the recursive projection method. *AIAA Journal*, 42(9):1765–1774, 2004.

[5] W. Clark and K. Hall. A time-linearized analysis of stall flutter. *Journal of Turbomachinery*, 122(3):467–476, 2000.

[6] S. S. Davis. Naca 64a010 (nasa ames model). oscillatory pitching. Technical Report AGARD-R-702, AGARD, 1982.

[7] R. Dwight. *Efficiency Improvements of RANS-Based Analysis and Optimization using Implicit and Adjoint Methods on Unstructured Grids*. PhD thesis, School of Mathematics, University of Manchester, 2006.

[8] R. Dwight and J. Brezillon. Effect of various approximations of the discrete adjoint on gradient-based optimization. In *Proceedings of the 44th AIAA Aerospace Sciences Meeting and Exhibit, Reno NV, AIAA-2006-0690*, 2006.

[9] R. Dwight, J. Brezillon, and D. Vollmer. Efficient algorithms for solution of the adjoint compressible Navier-Stokes equations with applications. In *Proceedings of the ONERA-DLR Aero Symposium*, 2006.

[10] T. Gerhold and M. Galle. Calculation of complex three-dimensional configurations employing the dlr tau-code. In *AIAA-97-0167*, AIA 1997.

[11] J. P. Giesing, T. P. Kalman, and W. P. Rodden. Direct application of the nonplanar doublet lattice method. In *Subsonic Unsteady Aerodynamics for General Configurations*, volume **I**, pages 279–285. AFFDL, February 1971.

[12] A. K. Gopinath and A. Jameson. Time spectral method for periodic unsteady computations over two- and three- dimensional bodies. In *43rd AIAA Aerospace Sciences Meeting and Exhibit*, Reno, Nevada, January 10-13 2005.

[13] S. Görtz and J. Möller. Evaluation of the recursive projection method for efficient unsteady turbulent cfd simulations. *24th International Congress of the Aeronautical Sciences, ICAS 2004*, 2004.

[14] A. Griewank. *Evaluating Derivatives, Principles and Techniques of Algorithmic Differentiation*. Number 19 in Frontiers in Appl. Math. SIAM, Philadelphia, 2000. ISBN 08-987-1451-6.

[15] K. Hall and W. Clark. Linearized Euler predictions of unsteady aerodynamic loads in cascades. *AIAA Journal*, 3(31):540–550, 1993.

[16] K. Hall, W. Clark, and C. Lorence. A linearized Euler analysis of unsteady transonic flows in turbomachinery. *Journal of Turbomachinery*, 116(3):477–488, 1994.

[17] D. Hoyniak and W. Clark. Aerodynamic damping predictions using a linearized Navier-Stokes analysis. In *ASME Paper 99-GT-207*, 1999.

[18] A. R. Hübner, A. Bergmann, and T. Löser. Experimental and numerical investigations of unsteady pressure distributions and aerodynamic forces on moving transport aircraft configurations. In *47th AIAA Aerospace Sciences Meeting*, volume AIAA-2009-0091, Orlando, Florida, 2009.

[19] S. Lu and R. Voss. Tdlm - a transsonic doublet lattice method for 3d potential unsteady transonic flow calculation. FB 92-25, Deutsche Forschungsanstalt für Luft- und Raumfahrt, 1992.

[20] G. Mortchéléwicz. Application des equations d'euler linearisees a la prevision du flottement. Technical Report AGARD-R-822, AGARD, 1998.

[21] W. Ning, Y. Li, and R. Wells. Predicting blade-row interactions using a multistage time-linearized Navier-Stokes solver. *Journal of Turbomachinery*, 125(1):25–32, 1998.

[22] A. Pechloff and B. Laschka. Small disturbance navier-stokes method: Efficient tool for predicting unsteady air loads. *Journal of Aircraft*, **4**3(**1**):17–29, 2006.

[23] Y. Saad. *Iterative methods for sparse linear systems*. Self published, 2000.

[24] Y. Saad and M. H. Schultz. GMRES: A generalized minimum residual algorithm for solving non-symmetric linear systems. *SIAM Journal of Scientific and Statistical Computing*, 7(3):856–859, 1988.

[25] G. M. Schroff and B. Keller. Stabilization of unstable procedures: The recursive projection method. *SIAM Journal of Numerical Analysis*, 30(4):1099–1120, August 1993.

[26] D. Schwamborn, T. Gerhold, and R. Heinrich. The dlr tau-code: Recent applications in research and industry. In *ECCOMAS CFD 2006*, TU Delft, The Netherlands, 2006.

[27] P. R. Spalart and S. R. Allmaras. A one-equation turbulence model for aerodynamic flows. Aiaa paper 92-0439, AIAA, 1992.

[28] C. Weishäupl and B. Laschka. Small disturbance euler-simulations for unsteady flows of a delta wing due to harmonic oscillations. *Journal of Aircraft*, 41(4):782–789, 2004.

[29] R. J. Zwaan. Lann wing: Pitching oscillation. data set 9. Technical report, AGARD-R-702, 1985.